ARL-TR-8055 ● JULY 2017

US Army Research Laboratory

Magneto-Hydrodynamic Simulations of a Magnetic Flux Compression Generator Using ALE3D

by George B Vunni

NOTICES

Disclaimers

The findings in this report are not to be construed as an official Department of the Army position unless so designated by other authorized documents.

Citation of manufacturer's or trade names does not constitute an official endorsement or approval of the use thereof.

Destroy this report when it is no longer needed. Do not return it to the originator.

ARL-TR-8055● JULY 2017

US Army Research Laboratory

Magneto-Hydrodynamic Simulations of a Magnetic Flux Compression Generator Using ALE3D

by George B Vunni
Weapons and Materials Research Directorate, ARL

REPORT DOCUMENTATION PAGE

Form Approved
OMB No. 0704-0188

1. REPORT DATE *(DD-MM-YYYY)*	2. REPORT TYPE	3. DATES COVERED
July 2017	Technical Report	October 2016–May 2017

4. TITLE AND SUBTITLE
Magneto-Hydrodynamic Simulations of a Magnetic Flux Compression Generator Using ALE3D

5a. CONTRACT NUMBER

5b. GRANT NUMBER

5c. PROGRAM ELEMENT NUMBER

6. AUTHOR(S)
George B Vunni

5d. PROJECT NUMBER

5e. TASK NUMBER

5f. WORK UNIT NUMBER

7. PERFORMING ORGANIZATION NAME(S) AND ADDRESS(ES)
US Army Research Laboratory
ATTN: RDRL-WMP-D
Aberdeen Proving Ground, MD 21005-5066

8. PERFORMING ORGANIZATION REPORT NUMBER
ARL-TR-8055

9. SPONSORING/MONITORING AGENCY NAME(S) AND ADDRESS(ES)

10. SPONSOR/MONITOR'S ACRONYM(S)

11. SPONSOR/MONITOR'S REPORT NUMBER(S)

12. DISTRIBUTION/AVAILABILITY STATEMENT
Approved for public release; distribution is unlimited.

13. SUPPLEMENTARY NOTES

14. ABSTRACT
Magnetic flux compression is a proven technique for the generation of ultrahigh magnetic fields, large currents, and large energy densities. The intent is to supply a few mega-amperes of seed-current for a fast high current when large capacitor banks are not available. A magnetic flux device consists of coils surrounding a cylindrical armature where an explosive drives the armature radially and causes a drop in the inductance. In this report, the results of ALE3D magneto-hydrodynamic simulation of a magnetic flux compression generator designed by the US Army Research Laboratory are presented. The simulation results are compared with the experimental data from 3 experiments with identical generators but different seed-currents. The simulation results show good agreement.

15. SUBJECT TERMS
magnetic flux compression, ALE3D, magneto-hydrodynamics, MHD, simulation, seed-current

16. SECURITY CLASSIFICATION OF:			17. LIMITATION OF ABSTRACT	18. NUMBER OF PAGES	19a. NAME OF RESPONSIBLE PERSON
a. REPORT	b. ABSTRACT	c. THIS PAGE			George B Vunni
Unclassified	Unclassified	Unclassified	UU	28	19b. TELEPHONE NUMBER (Include area code) 410-278-8538

Contents

List of Figures

Acknowledgments

The author would like to thank Dr Robert L Doney and John Runyeon for useful comments and suggestions. The author would also would like to thank Dr Casey Uhlig and Peter Bartkowski for peer reviews of this work. Special thanks to Peter Bartkowski for making this work successful and providing the experimental data accompanying this report. Thanks also to Dr Anthony Johnson of Lawrence Livermore National Laboratory for lending his computational expertise and always being willing to have a technical discussion on modeling magnetic flux compression generators.

This work was supported in part by a grant of computer time from the Department of Defense High Performance Computing Modernization Program at the US Army Research Laboratory Department of Defense Supercomputing Resource Center.

INTENTIONALLY LEFT BLANK.

1. Introduction

Many advances in design, understanding, and performance of magnetic flux compression generators (MFCGs) have occurred since the concept of using high explosives to push a metal and compress a trapped magnetic field was first introduced.[1] In recent years, the US Army Research Laboratory (ARL) has been actively engaged in an experimental program using explosively driven MFCGs as pulsed-power sources for onboard Army vehicle platforms.[2] ARL's research on MFCGs was initially focused on experimental development. However, recently there has been a shift toward developing new experiments informed by computational models and simulations. Previous efforts in modeling MFC (2010–2012) using the 3-D ALEGRA magneto-hydrodynamic (MHD) code demonstrated continuous kinematics, current amplification, and answered questions regarding armature velocity on system performance, inductance scaling in helicoils, and how magnetic energy is partitioned among air, conductor, and explosive during compression. However, modeling a full device was prohibitive at the time due to the computational cost triggered by the then available magnetic boundary conditions.[3] This report presents the first successful simulation of ARL's MFCG using ALE3D-MHD code.[4]

The main objective of this work is to understand and analyze the mechanisms of ARL's MFCG. To accomplish this, simulations were conducted using the ALE3D-MHD multiphysics code developed by Lawrence Livermore National Laboratory (LLNL).[4] ALE3D is a multiphysics numerical simulation software tool using arbitrary Lagrangian-Eulerian (ALE) techniques.[4] The 3-D simulations were directly compared with experiments conducted at the ARL experimental facilities. The simulation results showed lower initial inductance but accurately predicted the current trace. Despite challenges to the 3-D MHD modeling, the complexity of the problem, and insufficient material conductivity models, the simulation result shows that ALE3D-MHD can provide useful insights into the generator operation that are otherwise unattainable from the experiment.

2. Technical Purpose and Benefits

Numerical 3-D MHD simulation is one of the tools used for detailed understanding of, and a quantitative description for, physical phenomena occurring in explosively driven MFCG. Simulation of ARL's current MFCG device could lead to an improvement in future designs and optimization. Matching measurable data to models is important for accurate validation.

3. Background

Explosively driven MFCGs are compact pulsed-power sources of current and voltage. The interest in such devices stems from their unique capability to achieve very high energy densities, magnetic field strengths, and high current pulses. In a typical MFCG, a flux is established in a system of conductors arranged such that the magnetic flux is trapped. The system is explosively deformed to a smaller volume, thus compressing the magnetic flux and delivering electromagnetic energy into the connected load.[1,5] Compression of the trapped magnetic flux amplifies the initial seed-current (established by a small capacitor bank) injected into the coil. During this process, the inductance of the device rapidly decreases. In most MFCG devices the energy density (i.e., the ratio of the electrical energy delivered to the load and the MFCG volume) is typically a few joules per cubic centimeter.

The combination of high energy density and an operation on the microsecond time scale make the MFCG an excellent choice as part of a pulsed-power system. The tradeoff for the superior energy density of MFCGs compared with conventional pulsed-power sources is the single use nature of MFCGs.

Figure 1 illustrates a 3-D cutaway diagram, which shows the generator and the load section of a typical ARL-designed MFCG.[2] The generator has a length of about 432 mm and an outer diameter of 114.30 mm. The initial inductance was approximately 2955 nH, and the final inductance was approximately 160 nH. The stator consisted of a helical coil machined from a seamless 6063-T6 aluminum tube. The coil was designed to have nine turns over 203.2 mm of axial length.

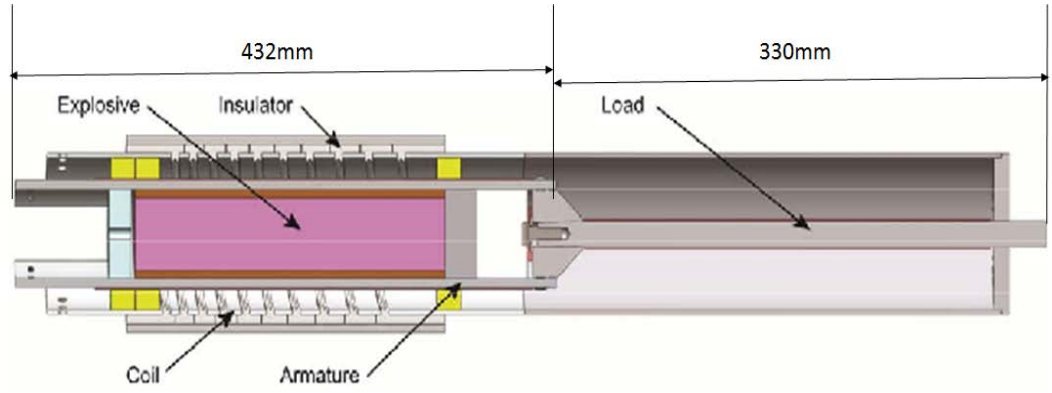

Fig. 1 A cross-sectional view of MFC showing the generator and the load[2]

The armature, a hollow metal tube filled with high explosive, was machined from a 6061-T6511 aluminum tube with an outer diameter of 7.62 cm. This yields an armature expansion ratio (final radius: initial radius) of 1.42 and an initial and final wall thickness of 6.4 and 4.5 mm, respectively. The explosive charge consisted of

a paper reinforced phenolic cylinder filled with Comp-B explosive. The phenolic cylinder was 25.0 cm long with an outer diameter of 6.35 cm. The Comp-B explosive charge filled the interior volume of a 5.08-cm diameter. The initial seed-current was supplied through copper stripeline from a 533-µF capacitor bank. The total inductance was 2955 nH with the load accounting for 160 nH, resulting in a theoretical lossless gain of 18.5.

Measured current profiles for seed-currents of 70 kA, 117 kA, and 220 kA are shown in Fig. 2, with peak-amplified currents of 414 kA, 714 kA, and 1.044 MA, respectively.[2] This represents current gains of 5.91, 6.10, and 4.73, respectively.[2] The MFCG did not perform as well as predicted with respect to overall theoretical gain. The average gain for the 3 tests was 5.56 compared to a theoretical gain of 18.5. Observation of the current plots reveals compression lasting for approximately 20 µs.

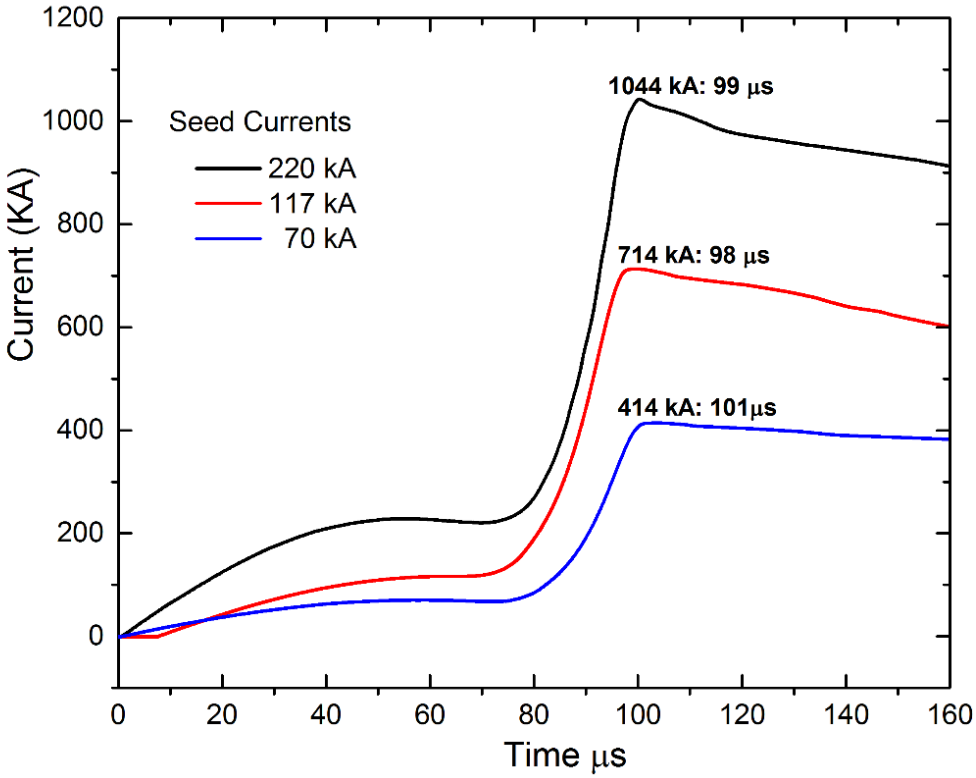

Fig. 2 Experiment current profiles for seed-currents of 70, 117, and 220 kA

4. Computational Model of ARL's MFCG Device for MHD Simulation

Simulations were performed using ALE3D-MHD, a 3-D multiphysics numerical simulation software tool using ALE techniques developed by LLNL.[4] ALE3D's MHD model is capable of capturing the dynamics of electrically conducting solids and fluids. The MHD module was developed for the modeling of coupled electro-thermal-mechanical systems that are inherently 3-D in nature.

The ALE3D-MHD module solves the resistive magnetic induction equation given a collection of specified current and voltage sources. The equation is solved in the Lagrangian frame using a mixed finite element method employing $\nabla \times H$ and $\nabla \cdot H$ finite element basis functions, which preserves the solenoidal nature of the magnetic field. Electromagnetic force and resistive joule heating terms are coupled to the equations of motion and thermal diffusion in an operator split manner.[4] For problems that require mesh relaxation (explosively driven MFCGs), magnetic advection is performed using the method of algebraic constrained transport that is valid for unstructured hexahedral grids with arbitrary mesh velocities. The advection method maintains the divergence-free nature of the magnetic field and is second-order accurate in regions where the solution is sufficiently smooth. For regions in which the magnetic field is discontinuous (e.g., MHD shocks), the advection step is limited using the method of algebraic flux correction, which is local extremum diminishing and divergence preserving. Details pertaining to the ALE3D-MHD can be found in Anderson et al.[4]

Figure 3 shows the MFCG material configuration used in the simulation, which was simplified by eliminating several components not significant to the physics investigated in the simulation. For example, it was not necessary to include the front-end explosive tamper (which is to diminish the resistive flux loss). Additionally, the capacitor bank and associated cables were not modeled directly, instead a direct current source applied to input region was applied. Unlike in the experiment, the seed-current was ramped from zero to its nominal value in 1 μs, kept flat for 20 μs, and then ramped back to zero. To reduce computational time, the seed-current was adjusted so that crowbarring (armature touching the crowbar and isolating the seed-current) occurred at approximately 6.5 μs. A further simplification included the use of copper rather than brass as reported in Bartkowski and Berning[2] for the crowbar (a metallic cylindrical conductor used to short out the seed-current and trap the magnetic flux in the shrinking volume between the coil and armature). The material geometry shown in Fig. 3 was generated in Cubit[6] using Python scripts,[7] and each component was exported as a tetrahedral mesh that was used for shaping materials into ALE3D. Material

equation-of-state (EOS) electrical and thermal conductivity models were taken from the ALE3D material database.[4] Tabular EOSs were made available through ALE3D's interface to LLNL's SESAME data.[8]

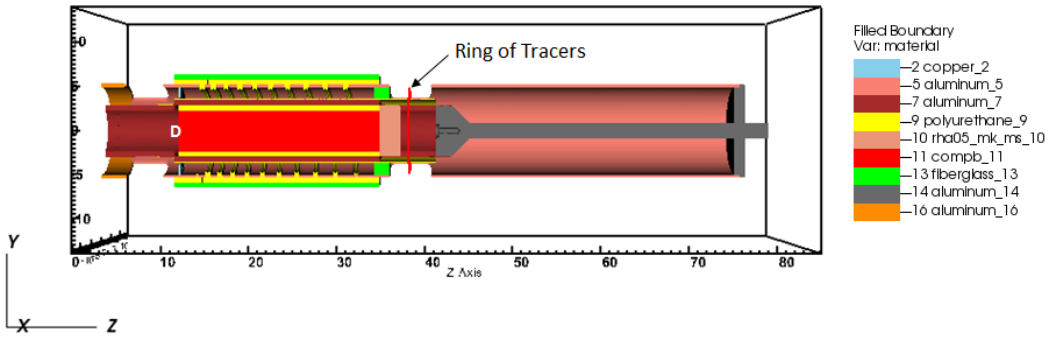

Fig. 3 Half-plane view of the geometry used in ALE3D simulation showing the materials

There are 2 broad approaches to modeling in ALE3D. A mesh that conforms to the structural elements in the system generally gives the most accurate simulation, but creating this type of mesh can be time-consuming. Since MFCGs have a cylindrical geometry, a high-resolution mesh is not required; one can use a conformal mesh and paint (shape) the actual geometries onto the mesh, allowing mesh elements to intersect the user-defined shape. The mesh was defined by a built-in function of ALE3D. Symmetry and magnetic boundary conditions were applied at z = 0. All other boundaries have outflow boundary conditions. The high explosive was initiated at t = 0 at point label "D" (x, y, z) = (0, 0, 9.53 cm) shown in Fig. 3. A direct current source was applied to the input region connecting the front end of the armature and the coil.

The compressed current diagnostics is critical for comparing the simulation results with the experiment. It is one of the most important quantities of the simulation to predict magnetic compression in the MFCG discharge. In the simulation, the current was measured by introducing a 360° ring of B-field tracers around the output as illustrated in Fig. 3. The orientation was such that B-field tracers follow the direction of the magnetic field along the vector line of the ring allowing it to measure accurately the compressed current. From the generated time histories of the magnetic field B, an element of the tracer length was integrated over the loop using Ampère's law given by

$$\oint \vec{B} \cdot \vec{dl} = \mu_o I_{enc} , \quad (1)$$

which was used to calculate the current enclosed by the line integral. A postprocessing Python script written by Anthony Johnson[9] of LLNL and modified

by this author, converted the B-field data into a current inside the ring, effectively simulating a Rogowski coil placed around the load.

5. Simulation Results: Computational Mesh Convergence

One of the key aspects of numerical simulation is the effect of mesh resolution on a given parameter of interest. Simulations require adequate resolution to ensure convergence of the solution. If the mesh resolution is too coarse, numerical errors may become significant and physically important features may not be resolved. To check for numerical convergence of the current, 4 computational cases were run (using the 70-kA seed-current), varying the number of elements. For each case, the current-time history is plotted and compared with the experimental data. The results of this convergence study are shown in Fig. 4. The simulation is time shifted and overlaid on top of the experimental plot. In general, (for all mesh resolution) the current plots match well for the first 20 μs and then slightly overshoot the experimental current.

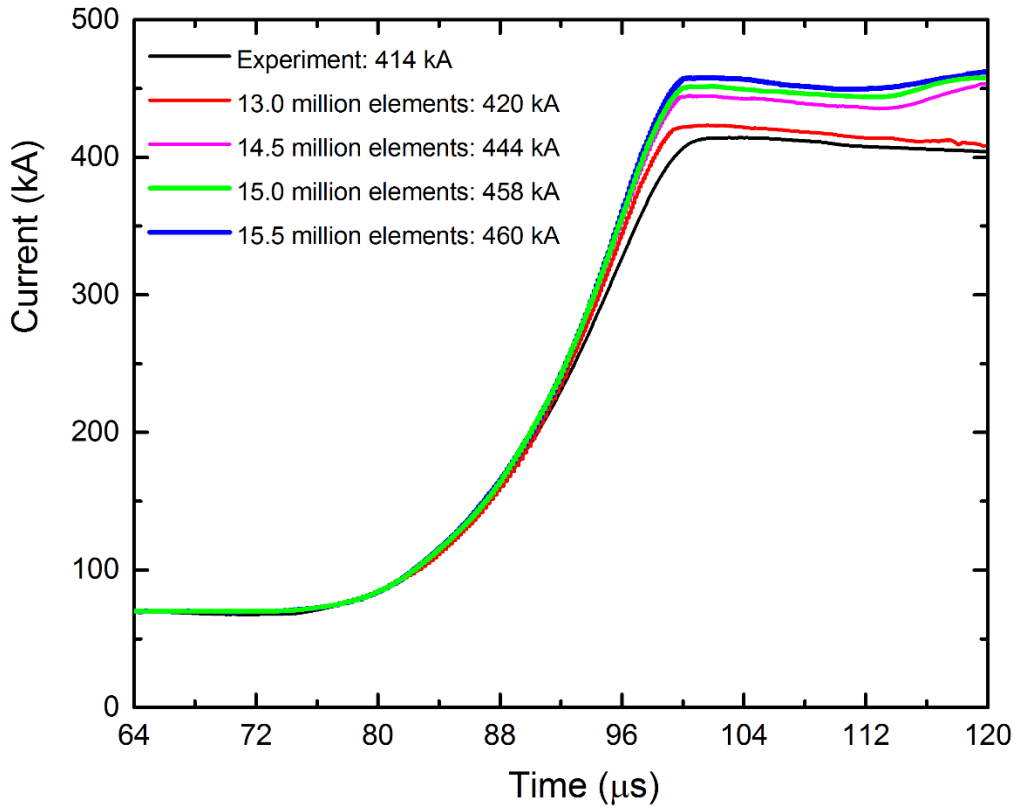

Fig. 4 Impact of mesh resolution on the current amplification for 70-kA seed-current

The low resolution (element count of 13 million) resulted in a maximum current of 420 kA that is 1.4% more than the experimental value. At higher resolutions (element count of 14.5–15 million), the calculated maximum current begins to converge at 7–11 % higher than the measured value. These convergence tests are on the same length scale as the real problem, and both the low and high resolution consumed approximately the same computational resource (i.e., time, number of cores).

The results of the convergence simulations indicate that the compressed current is sensitive to element size and evaluation of $\vec{J} \times \vec{B}$ coupled to the equation of motion. The EOS and the nonlinear relationship between the electrical conductivity and the joule heating may also influence the magnetic flux at the end of the compression, thus increasing the compressed current (current was derived from the B-field using Ampère's law). In addition, the change in electrical conductivity produced by the shock wave from explosive loading of the armature, arcing, and stray magnetic flux is not considered in this simulation, and it was neglected in calculating the compressed current. Further analysis will help with understanding the increase of the magnetic flux with mesh resolution at the end of the compression. For simulations using the 117- and 220-kA seed-current, mesh density of 14.5 million elements was used.

6. Comparison of ALE3D Simulation with Experiment

Figure 5 shows the current profiles from ALE3D-MHD simulations and experiments for 117- and 220-kA seed-currents. Similar to Fig. 4, the agreement between simulation and experiment is reasonable up to a few microseconds before the peaking of the current. For the 220-kA seed-current, the simulation predicted a maximum current of 1213 kA, which differs from measured peak current of 1044 kA by 16%. For the 117-kA seed-current, the maximum current was overpredicted by 4%.

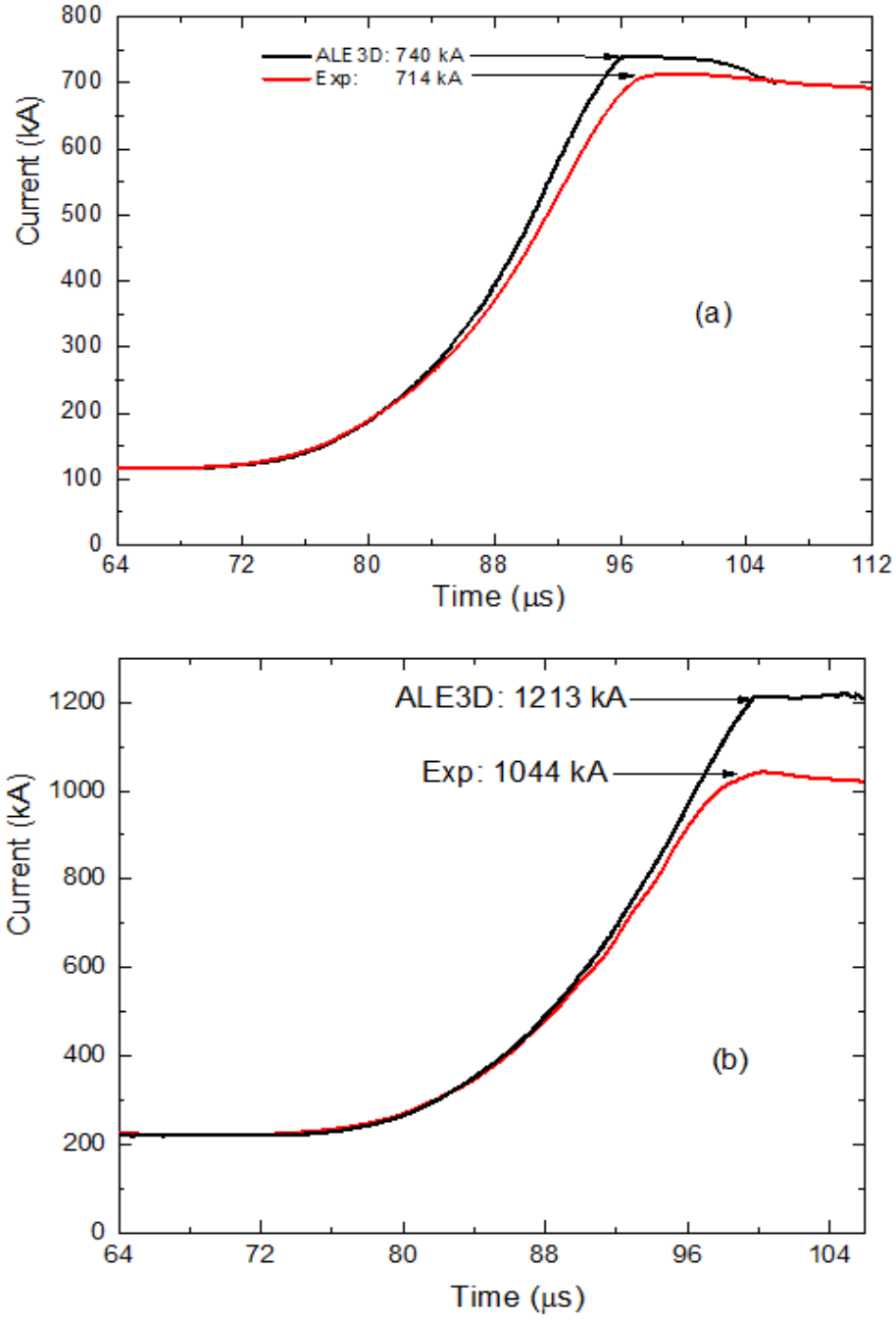

Fig. 5 Comparison of ALE3D-MHD simulation (black line) and experimental current trace (red line) for a) 117- and b) 220-kA seed-currents. The simulation is shifted 62 μs to account for the delay in the experiment.

The time-varying inductance of the device is a critical point of the simulation. Deviations from the actual inductance value will lead to a mismatch of theory and experiment in the temporal current waveform. Since most of the action (i.e., high current amplitude) occurs toward the end of generator operation, typically during the last 10 μs, the inductance calculation needs to be especially accurate for these last moments before generator burnout. Figure 6 shows a plot of calculated and measured inductance.

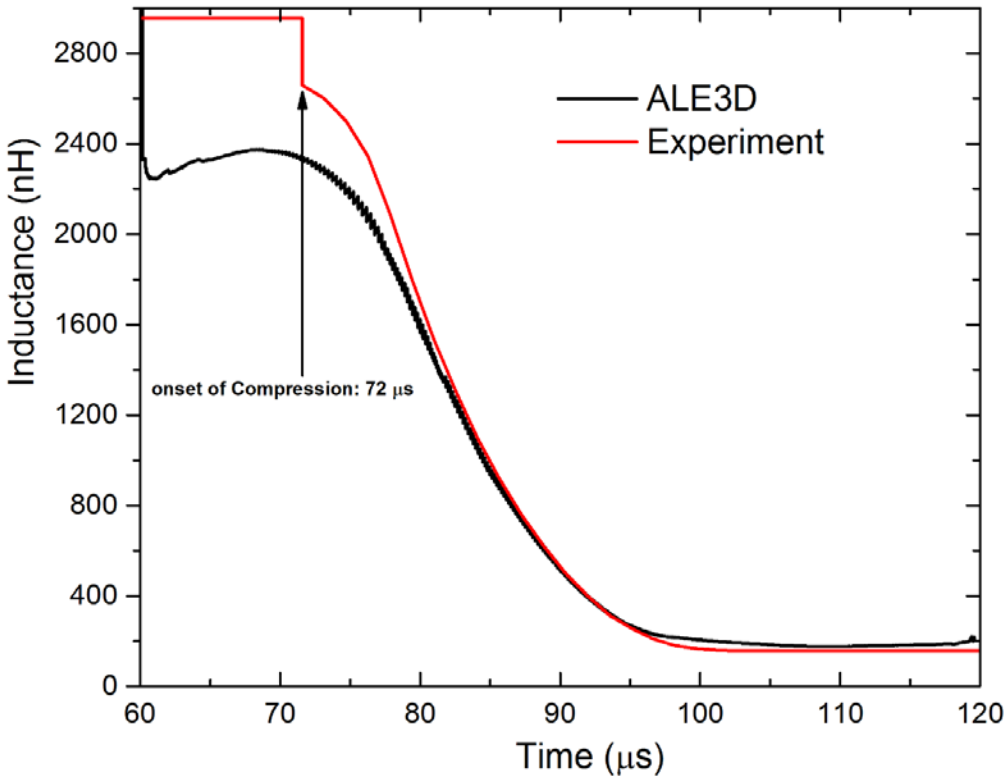

Fig. 6 Comparison of the simulated and measured inductance evolution

The time history of the simulated inductance compared with the measured inductance in Fig. 6 is somewhat puzzling during the early portion of the experiment. The measured static inductance (~2900 nH) differs significantly from the ALE3D simulation (~2300 nH). At late times (end of compression), the agreement with the experiment is quite good. The differences may be explained by the method used in deriving the inductances. In the simulation, the dynamic inductance was derived from the magnetic energy that is extracted from the time history of the scalar circuit current (the magnetic energy is only correct for materials with constant value of permeability). However, it is difficult to accurately measure the time variations of the inductances during the detonation. The experimental inductance was measured in the laboratory using a meter. The measurement was

performed with a conical sliding insert resembling the armature movement inside the stator.[2] The time history of the inductance was then calculated using the detonation velocity of the explosive.

Figure 7 shows the total magnetic field strength of the generator, scaled by the initial field strength from the seed-current. The peak magnetic field strength of 1.2 MegaGauss (MG) or 120 tesla (T), 0.4 MG (40 T), and 0.1 MG (10 T) were obtained for seed-currents of 220 kA, 117 kA, and 70 kA, respectively. These values should be compared with experimental values in the future.

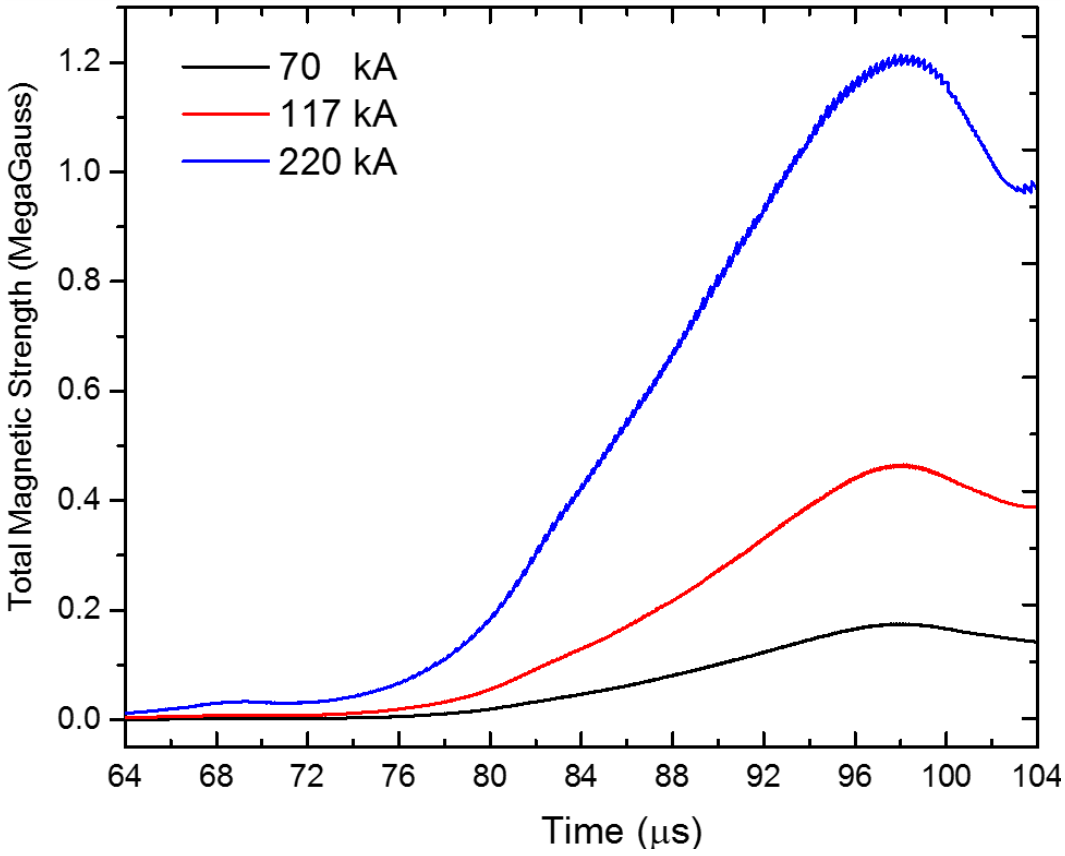

Fig. 7 Generator total magnetic strength for 70-, 117-, and 220-kA seed-currents

Figure 8 shows typical snapshots of the magnetic flux during current compression, indicating the increase in field strength. The unique feature of the generator is shown in the last snapshot, where the magnetic flux has been transferred from the coil on the right to the load on the left.

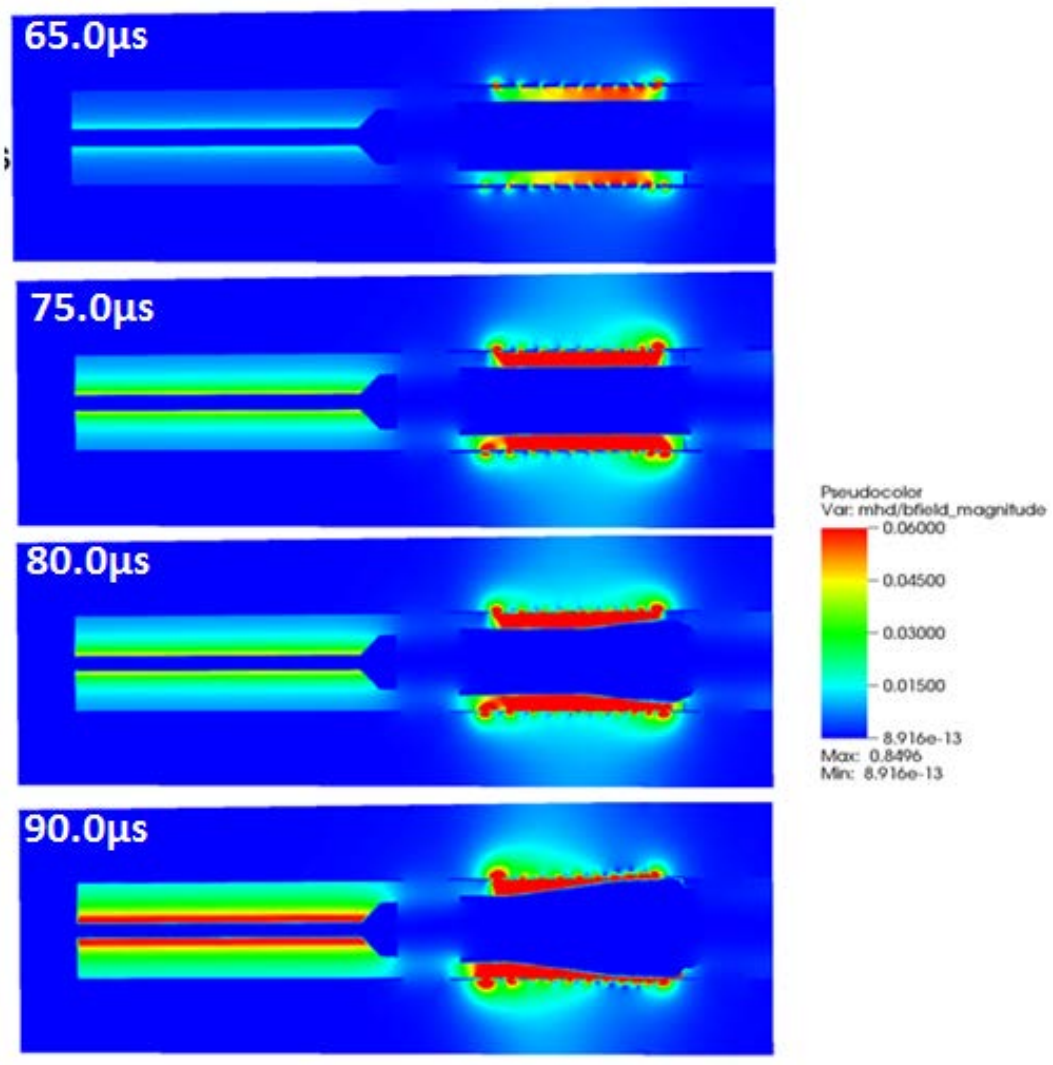

Fig. 8 Snapshots of the generator magnetic flux magnitude at 65, 75, 80, and 90 µs

7. Analysis of Simulation: Flux Compression Principle

The current gain of a generator (G) is defined by the ratio of initial to final inductance. Theoretically, the larger the initial inductance (L_i) and the smaller the final (load) inductance (L_f), the more gain is expected. Of course, our assumption of ideal flux conservation cannot hold true for a real system, as we will always have ohmic losses in the conductors and other intrinsic flux losses. However, by adding a figure of merit (β), we can write

$$G = \left(\frac{L_i}{L_f}\right)^{\beta} \tag{2}$$

for an ideal generator β = 1.0. For experiments reported in Bartkowski and Berning,[2] the average value of β = 0.62 compared to the average simulation value of 0.77.

Figure 9 shows the armature expansion angle. The armature will expand in a conical shape with an angle determined by the ratio of the mass of the aluminum tube to the mass of high explosives. Figure 9 shows a snapshot of the expanding armature 22 μs after initiation of the high explosive. The contact point between the armature and stator is at position A (z = 173 mm, r = 50 mm), and the tube begins to move at position B (z = 230 mm, r = 34.8 mm). The expansion angle is defined as the angle of the line between the 2 points A and B relative the generator axis. The angle α is calculated according to

$$\alpha = \arctan\left(\frac{50-34.8}{230-173}\right) = 14.9^{\circ}, \quad (3)$$

which is close to the calculated (using Gurney equations) value of 15.2° reported in Bartkowski and Berning.[2]

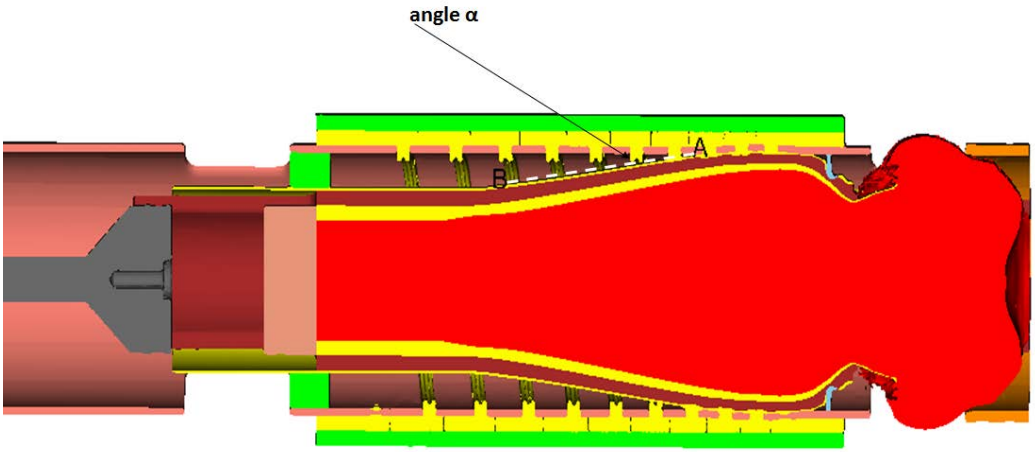

Fig. 9 Snapshot of the expansion angle of the armature

Deformation and Kinematics of Armature

The simplest way to look at an expanding armature is to think of it as having the consistency of butter, in which case the resting crowbar will cut through the armature just like a knife through butter. This is indeed the case, as the image in Fig. 9 reveals (crowbar is light blue, right-hand side of image). In Fig. 10, a plot of the radial displacement history of a point on the armature located at the axial position of 122 mm. The dip in the plot (the point marked with a letter A) is due to the crowbar cutting into the armature.

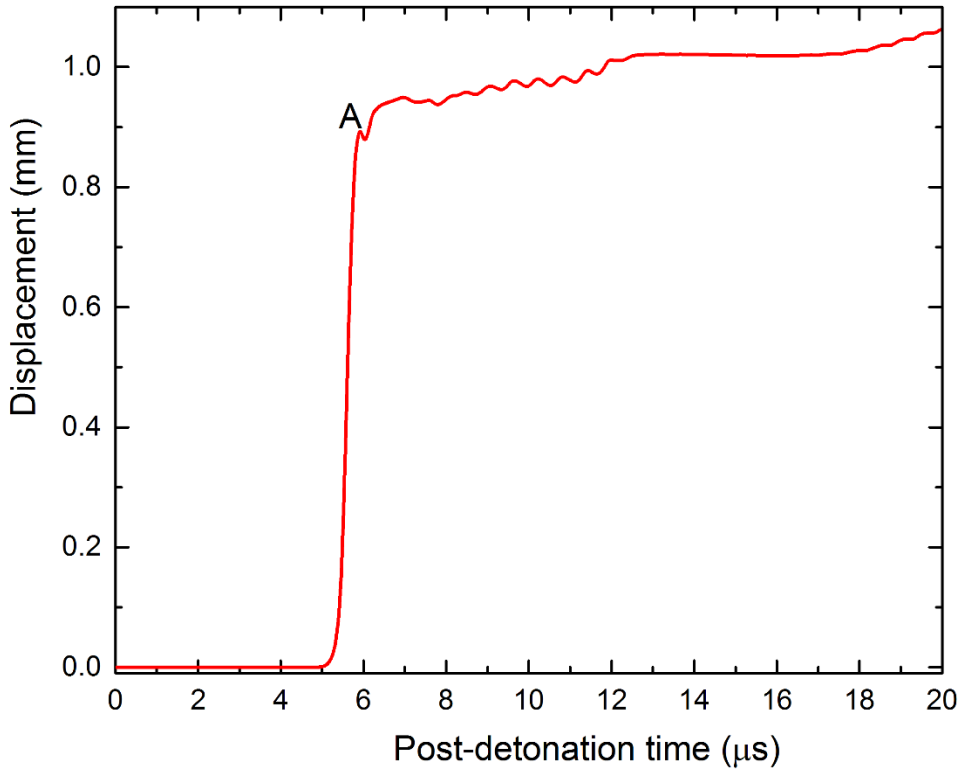

Fig. 10 Radial displacement of a point close to the armature at the axial position of 122 mm

The radial expansion history of the armature at 25 μs (after detonation) and images of the expanding armature are shown in Figs. 11 and 12. The measured armature expansion is also shown. Letter "A" marks the point of crowbar impact caused by the downward spike. The simulation result shows the end-effect (a bell-shaped contour of the armature at the detonation side).[1] This behavior is attributed to the fact that in MFCGs the detonation end is normally open to outside air. When the explosive is detonated, some of the detonation pressure escapes through the open end, which in turn reduces the outward expansion of the armature at this location.

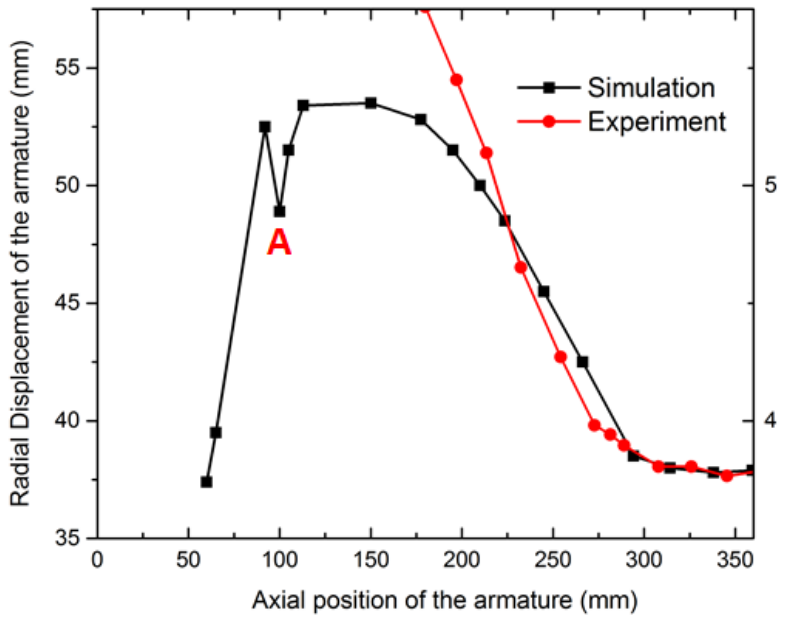

Fig. 11 Radial displacement of the armature at 25-μs postdetonation time

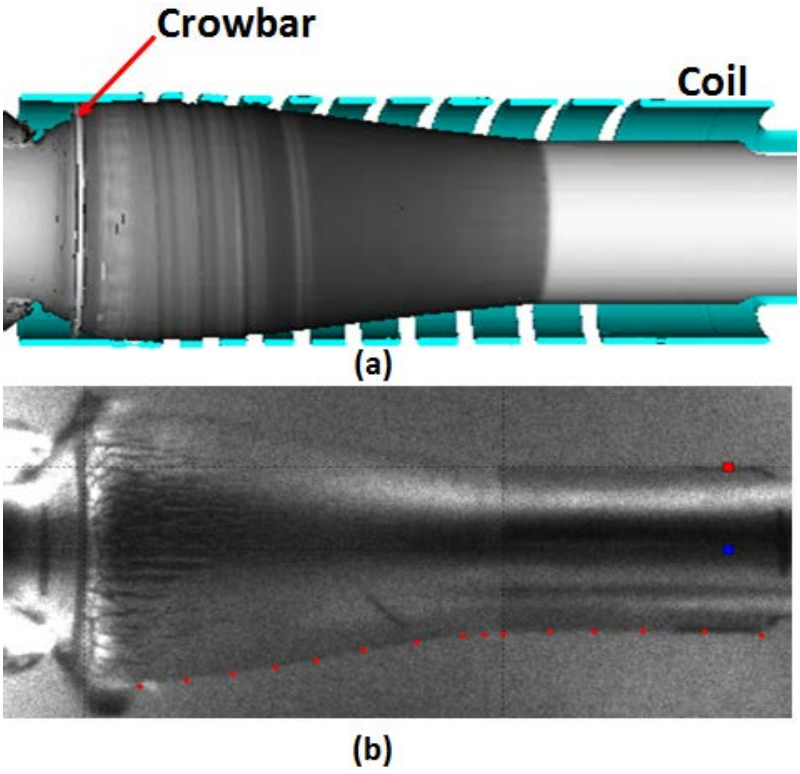

Fig. 12 Qualitative comparison of the expanding armature at 25 us (after detonation): a) ALE3D simulation and b) experiment. Coil and crowbar are shown in the simulation image.

Away from the detonation point, the experimental measurements and ALE3D simulations of the armature expansion agree but differ at the detonation point. The difference is explained because the experimental data were calculated from expansion of the armature only (no crowbar and stator, allowing the armature to expand freely unlike in the simulation). The most important conclusion to be drawn from the comparisons is that the radial expansion is in excellent agreement away from the detonation point.

8. Conclusion

In this work, the results of a 3-D numerical study of the ARL-designed MFCG using ALE3D-MHD code from LLNL are presented. Results of 3-D ALE3D simulations of the MFCG were compared with the experimental data and show good agreement at low-mesh resolution (a 1.4% difference). However, at high-mesh resolution, the code overpredicted the compressed current by 7–14%. There is also good agreement of the inductance and armature expansion. In the simulation, arcing, stray magnetic flux, nonlinearity in the conductivity model, and magnetic pressure was neglected. The comparison of ALE3D results with the well-diagnosed experiments indicates that the code is capable of giving accurate results until the end of the compression.

9. Recommendations for Future Work

Some areas of the magnetic flux compression have not been studied; it would be considerably relevant in understanding potential experimental improvements. Future continued modelling will include the following areas, as they have not been studied:

- Perform deeper analysis of magnetic forces inside the generator.
- Calculate magnetic losses due to switching flux, electrical breakdown, resistive heating, and temperature of the materials during flux compression.
- Test the model with transition reduction elements in ALE3D code (a mechanism for putting a mesh where it is needed, and a method of creating elements with one number of faces on one side and a different number on the opposing side).
- Conduct simulations using lumped circuit model for the seed-current. This may increase the computational time, but it is of particular value for predictive modeling.
- Investigate breakdown that occurs in the compression phase.

- Investigate possible effects due to electromagnetic forces acting inside the generator. For example for high currents, the rotational effect of the armature produced by the electromagnetic forces.

10. References

1. Neuber AA. Explosive driven pulsed power: helical magnetic flux compression generators. Berlin (Germany): Springer; 2005.

2. Bartkowski P, Berning P. Design and testing of the ARL squeeze 4 helical flux compression generator. Aberdeen Proving Ground (MD): Army Research Laboratory (US); 2013 June. Report No.: ARL-TR-6477.

3. Doney RL, Bartkowski P. Magnetic flux compression simulations using ALEGRA. Aberdeen Proving Ground (MD): Army Research Laboratory (US); 2012 July. Report No.: ARL-RP-384.

4. Anderson A, Barton N, Biagas K. User manual for ALE3D, an arbitrary Lagrange Eulerian system. Version 4.24. Livermore (CA): Lawrence Livermore National Laboratory; 2014 Sep 5.

5. Shearer JW, Abraham FF, Aplin CM, Benham BP. Explosive-drive magnetic field compression generators. J Appl Phys. 1968;39:2102–2116.

6. Morris R. Cubit 13.2 user documentation. Albuquerque (NM): Sandia National Laboratories; 2017.

7. Reitz K. Python guide documentation. Release 0.01. Wilmington (DE): Python Software Foundation; 2017 May 1.

8. Lynon SP, Johnson JD. SESAME, The Los Alamos National Laboratory equation of state database. Los Alamos (NM): Los Alamos National Laboratory; 1992. Report No.: LA-UR-92-3407.

9. Johnson AJ. Lawrence Livermore National Laboratory, Livermore, CA. Personal communication, 2016 Oct.

List of Symbols, Abbreviations, and Acronyms

3-D	3-dimensional
ALE	arbitrary Lagrangian-Eulerian
ARL	US Army Research Laboratory
EOS	equation-of-state
LLNL	Lawrence Livermore National Laboratory
MFCG	magnetic flux compression generator
MHD	magneto-hydrodynamic

1 (PDF) DEFENSE TECHNICAL INFORMATION CTR DTIC OCA

2 (PDF) DIRECTOR US ARMY RSRCH LAB RDRL CIO L IMAL HRA MAIL & RECORDS MGMT

1 (PDF) GOVT PRINTG OFC A MALHOTRA

1 (PDF) SNL J NIEDERHAUS

18 (PDF) DIR USARL
RDRL WMP A
P BERNING
C UHLIG
M COPPINGER
J FLENIKEN
RDRL WMP D
G B VUNNI
R DONEY
S SCHRAML
D KLEPONIS
D KEELE
C RANDOW
J RUNYEON
F MURPHY
RDRL WMP E
P BARTKOWSKI
D HORNBAKER
M LOVE
P SWOBODA
J HOUSKAMP
C KRAUTHAUSER

INTENTIONALLY LEFT BLANK.